EE665:Power Electronic Systems for EVs

Project Objective

DESIGHN, OPERATION AND CONTROL OF CAPACITIVE CHARGING CONVERTER

Under the Guidance

of

Dr. Chandan Kumar

Associate Professor., EEE Dept. IIT GUWAHATI

Final Draft

(Group No - 5)

Team Members and work done

- SHIVRAJ VISHWAKARMA - 224102112

  (LATAX Documentation, MATLAB Simulation, and some work in VSIO also)

- MAHENDRA PATEL - 224102107

  (Theoretical Analysis, Diagrams and figures in VSIO)

- ANKIT SINGH - 224102104
  (Circuit Diagrams in VSIO)

Capacitive Charging Converter

1. Introduction

Researchers continually strive to propose innovations for improving the comfort and safety of human existence in the midst of technological competition. Another component of it is wireless power transfer (WPT). Over a physical connection, WPT offers appealing advantages such as convenience, safety, and simplicity. WPT has been widely used in various applications over the past few years, including smartphone chargers, EV battery charging systems, and biomedical equipment[1]. One of the newest WPT approaches is capacitive power transfer (CPT). It is safer than other techniques and has a straightforward structure. However, the main problem with the capacitive transfer mechanism is that it loses a lot of efficiency as the load changes. our aim is to make a state-feedback (SF) controller

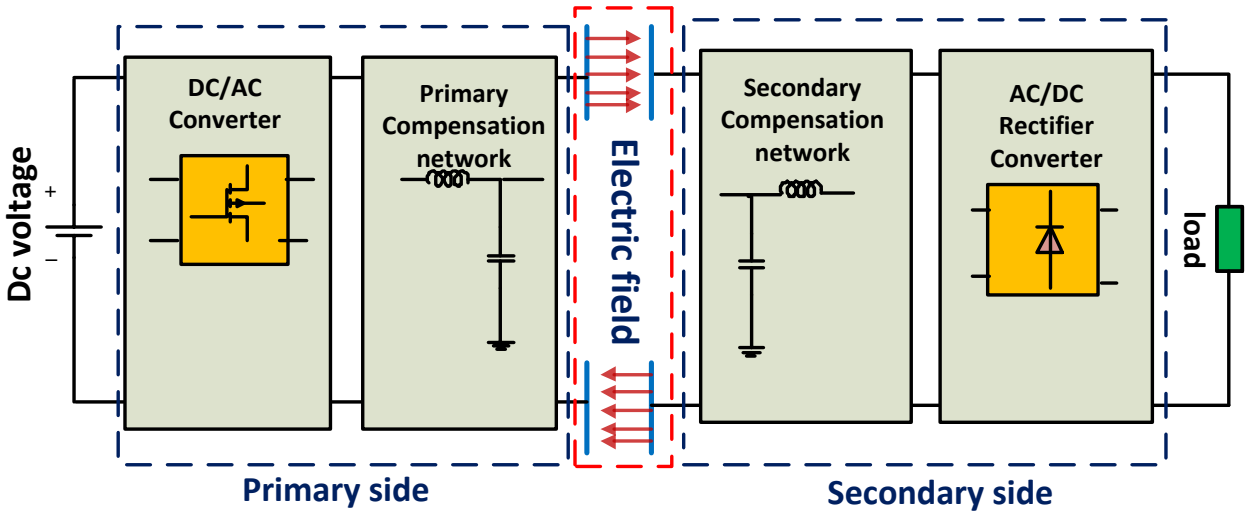

Figure 1: Block diagram of a general capacitive wireless power transfer system.

model that will keep the output voltage stable under fluctuating load conditions. As a result, despite fluctuations in load, the system's overall efficiency will be preserved. for that, The Generalized State Space Averaging (GSSA) method is used to create a mathematical model of the CPT system.

The coupling capacitors (Cs1, Cs2), the secondary side, and the primary side make up the three basic components of the CPT system. Based on the compensation topologies of both sides, the spacing between the coupling capacitors is determined.

In this study, a CPT system based on Series Resonant Converters (SRC) (a Class E inverter) that gives improved sensitivity to parameter fluctuation is described [2]. The primary purposes of a class E inverter are to create high-frequency switching and high power efficiency capabilities [3]. The

switching frequency must also be adjusted to maintain the system's output voltage in the face of changing circuit factors, such as the load. In order to provide a high-efficiency system, it is crucial to present a method that can change the switching frequency in response to load variation.

To analyze and comprehend the system's behavior, a mathematical model of the system was created. The Generalized State Space Average (GSSA) approach was employed to represent the CPT system since it has been demonstrated to be effective in simulating the SRC and satisfying the small ripple condition [4] [5] [6] [7] [8]. The Proportional-Integral (PI) and Linear Quadratic Regulator (LQR) controllers are the most often used controllers with the CPT system, while there are other controllers that may be used as well [9, 10]. However, not many controllers can provide quick changes in parameters. Designing SF controllers for the CPT system in order to maintain output voltage is the goal of this effort. To analyze and comprehend the system's behavior, a mathematical model of the system was created.

The structure of this report is as follows: In Section 2, the Class E power amplifier is presented and examined, while Section 3 extended on the development of the state space model for the CPT system.

2. ORIGIN OF THE CPT SYSTEM

Heinrich Hertz came up with the concept of this wireless technology in 1888 **[11]**. The electric field-linked wireless power transmission was successfully demonstrated by Nikola Tesla, the inventor of wireless power transfer, at Columbia University in New York as early as 1891. CPT was developed and used slowly at the time because to several limitations, including power electronics, electrical materials, and control technologies. The CPT system has been studied irregularly by academics from the United States, France, Singapore, and other nations since the 1960s. Some research results have been obtained, but the advancement has been very gradual. Due to the quick advancement of power electronics in recent years, CPT research and application have also grown significantly. After decades of development, the CPT system's transfer power, system efficiency, and transfer distance have all significantly increased. Currently, many WPT apps may be charged through the CPT system [12].

3. Basic Principle of CPT System [12]

Compared to the IPT system, research on the CPT system began much later. CPT applies an electric field to achieve power transfer as opposed to IPT, which uses a magnetic field as the transmission medium. IPT and CPT have dual relationships. The CPT system operates on the same fundamental tenet as IPT. Figure 2 depicts the overall circuit of the CPT system. A CPT coupler is created by

connecting two pairs of metal plates in series. As a channel for wireless power transfer, the coupling

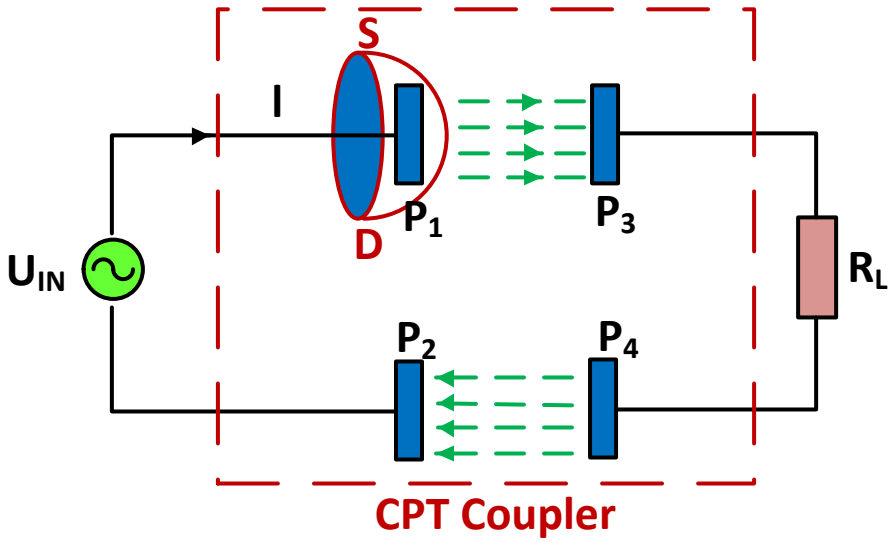

Figure 2: General CPT circuit with a simplified coupler

coupler is often made of copper or aluminum plates. Maxwell's full current theorem states that

$$\int_l Hdl = \int_S JdS + \int_S \frac{\partial D}{\partial t} dS \tag{1}$$

The total current flowing through the path's surrounding region S is equal to the line integral of the magnetic field strength H along any closed curve l. The conduction current flowing through the conductor is represented by the first component to the right of Equation (1), and J is the conduction current density. The displacement current, which is equivalent to the conduction current of the simultaneous circuit, is the second component in Equation (1). The displacement current density, or $\frac{\partial D}{\partial t}$, is the same as the rate of variation OF electric flux density D. The entire current theorem has the following differential form:

$$\Delta \times H = J + \frac{\partial D}{\partial t} \tag{2}$$

Equations (1) and (2) give a useful functional equation for the CPT system to quantitatively characterize how power is transported from plate P1 to P3 and explain the issue of discontinuous capacitive current from the micro viewpoint. The electric flux density between the electrode plates shifts to generate a displacement current. It achieves a wireless power transfer based on the CPT system when the electrode plates are subjected to alternating voltage excitation. Table 2 lists typical CPT resonant compensation topologies and their associated performances. Based on the requirements of actual application scenarios, several compensation topologies may be selected and created.

Table 2. Common resonant compensation topologies in CPT systems.					
Topologies	**Frequency**	**Power**	**Efficiency**	**Distance**	**Year**
LC-LC	1 MHz	216.5 W	52.2%	2000 mm	2019
LCL-LCL	1 MHz	1880 W	85.87%	150 mm	2016
LCLC-LCLC	1 MHz	2400 W	90.8%	150 mm	2015
CLLC-CLLC	1 MHz	2570 W	89.3%	150 mm	2021
LCLC-LC	893 kHz	96 W	84.636%	4 mm	2021
LC-CLC	800 kHz	2000 W	90.29%	150 mm	2020
LCL-L	1 MHz	1500 W	85.5%	150 mm	2020

4. CPT SYSTEM USING CLASS E INVERTER

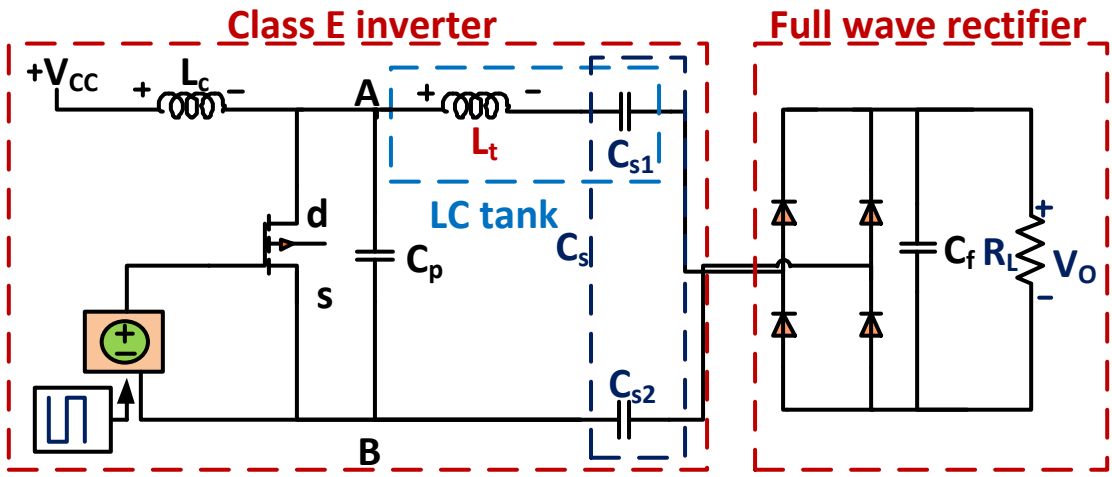

Figure 3: Schematic of the CPT system

”Fig. 3” depicts the planned CPT system’s schematic. The Class E inverter is connected to a full-wave rectifier. ”Fig. 4” shows the analogous circuit of the system. Re is the equivalent resistance of the loaded full wave rectifier, and resonant capacitor Cs is the equivalent of the series capacitors Cs1 and Cs2 [13]. Details of the computation were provided by [14] and [15].

$$C_s = \frac{C_{s1}C_{s2}}{C_{s1} + C_{s2}} \tag{3}$$

$$R_e = \frac{8}{\pi^2} R_l \tag{4}$$

To make the analysis simpler, the following presumptions were made [16]:

- The ideal switching MOSFET (zero on-resistance, infinity off resistance, and zero switching time)
- choke inductance, Lc, has a high enough value to supply current with little ripple. In other words, the input current's ac component is considerably smaller than its dc component.
- loaded quality factor, Q, of the resonate RLC circuit must be considered to be high enough to permit sinusoidal current, i_o through the resonant circuit.
- the switching duty cycle ratio, D, is 0.5.

The computation was carried out in accordance with [17] to acquire the values for the components depicted in "Fig. 4". The system's output power, Po, is determined using:

$$P_o = \frac{8}{\pi^2 + 4} \frac{V_{CC}^2}{R_e} \tag{5}$$

where Vcc is the dc supply voltage. In order to separate the resonant inductance, L_t, into its two

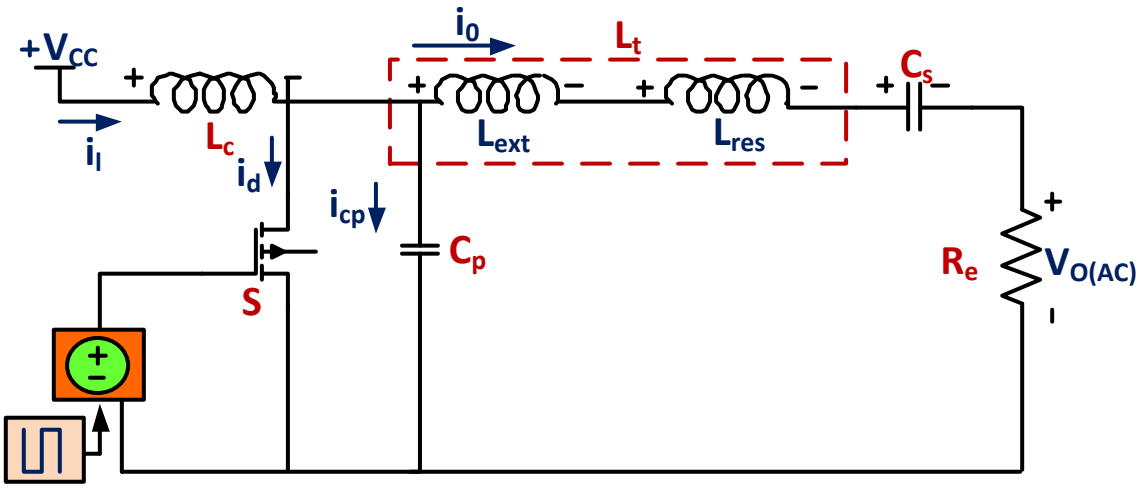

Figure 4: Equivalent circuit of the CPT system

components, L_{ext} and L_{res} were computed using:

$$L_t = L_{ext} + L_{res} \tag{6}$$

$$L_{ext} = \frac{1.153 R_e}{\omega} \tag{7}$$

$$L_{res} = \frac{Q R_e}{\omega} \tag{8}$$

where Q is the loaded quality factor and w is the switching frequency. The shunt capacitance, C_P is

given as

$$C_P = \frac{p_o}{\pi \omega V_{cc}^2} \tag{9}$$

we can compute the resonant capacitance, C_s, using

$$C_s = \frac{1}{\omega Q R_e} \tag{10}$$

the minimum value of the choke inductor, L_c, can be given as

$$L_{C(min)} = 2(\frac{\pi^2}{4} + 1)\frac{R_e}{f} \tag{11}$$

The drain voltage of MOSFET, V_{AB}, is given as:

$$V_{AB} = \left\{ \begin{array}{ll} \frac{I_o}{\omega C_p}[\omega t + \frac{3\pi}{2} - \frac{\pi}{2} cos\omega t - sin\omega t], & \text{if } \pi < \omega t < 2\pi \\ 0, & \text{if } 0 < \omega t < 2\pi \end{array} \right\} \tag{12}$$

6. MODELING OF THE CPT SYSTEM [1]

Figure 1 displays a simplified block diagram of a descriptive CPT system. Reactive networks on the primary and secondary sides are utilized for impedance matching between the source and load characteristics, much like magnetic field techniques. High-order matching networks are employed in any WPT system to obtain degrees of freedom in design, performance, and overall input-output connections. Such high-order networks might be difficult and complex to analyze. The complex relationship between the system parameters and attributes may as a result be disregarded or even missed. In order to understand how high-order resonant structures function, various techniques have been used, including geometrical representations, averaging, and the manipulation of analytical multivariable matrices. Clear closed-form expressions for the power delivery and other significant relationships are provided by the circuit derivation of the CPT by the super-positioning theorem. Accurate general descriptions, however, are not always achievable due to approximations, especially when describing dynamic properties. While numerical simulations are a powerful tool for assessing and describing various resonant circuits, they lose generality and can be time-consuming when a time domain cycle-by-cycle simulation is required. A straightforward and uniform State space modeling approach for capacitive-based WPT systems would be very helpful.

The main problem with the capacitive transfer mechanism is that it loses a lot of efficiency as the

load changes. As our aim is to make a state-feedback (SF) controller model that will keep the output voltage stable under fluctuating load conditions. As a result, despite fluctuations in load, the system's overall efficiency will be preserved. for that, The Generalized State Space Averaging (GSSA) method is used to create a mathematical model of the CPT system.

The suggested CPT system's mathematical model, shown in "Fig. 4," is discussed. Differential equations serve as the representative for the energy-storing components L and C. Resonance converters were modeled using the GSSA approach.

A. Large Signal Model of CPT System:

The large signal model is a technique for expressing the nonlinear signal in terms of the underlying nonlinear differential equations with regard to nominal time. The following differential equations were created using the CPT system's circuit and the Kirchhoff current law (KCL) and Kirchhoff voltage law (KVL) on the Class E inverter:

$$v_{AB} = L_t \frac{dI}{dt} + v_{cs} + sign(i)v_f \tag{13}$$

$$i = c_s \frac{dv_{cs}}{dt} \tag{14}$$

And, as follows, sgn(x) is the symbol function for the acceptable base wave approximation [18]:

$$sgn(x) = \left\{ \begin{array}{ll} 1, & \text{if } x > 0 \\ 0, & \text{if } x = 0 \\ -1, & \text{if } x < 0 \end{array} \right\} \tag{15}$$

As shown in the equation "(12)," v_{cs} is the voltage across the capacitors, I is the resonant current through the inductor, L_t, and v_{AB} is the voltage across the shunt capacitor. Similarly, the current going through the rectifier is determined by applying Kirchhoff's current law (KCL) as:

$$|i| = c_f \frac{dv_f}{dt} + \frac{v_f}{R_l} \tag{16}$$

The state vectors, i, v_{cs}, and v_f, were established from "(13), (14), and (15)". Despite being an energy-storing component, the shunt capacitor, Cp, is not regarded as a state variable since its dynamic behavior is entirely determined by the energy stored in the series capacitor, C_{cs}, and L_t.

The state variables are assumed to be the coefficients of the first-order Fourier series of each component's voltage and current signal. Therefore, the Fourier series expansion must be decomposed. It is

possible to simplify the Fourier series expansions of i(the series current flowing through L_t and C_s) and v_{cs} (the voltage applied to capacitor C_s) as:

$$\left.\begin{aligned} i &= i_s sin(\omega t) + i_c cos(\omega t) \\ v_{cs} &= v_s sin(\omega t) + v_c cos(\omega t) \end{aligned}\right\} \tag{17}$$

after differentiation equation (17) becomes:

$$\left.\begin{aligned} \frac{di}{dt} &= (\frac{di_s}{dt} - \omega i_c) sin(\omega t) + (\frac{di_c}{dt} + \omega i_s) cos(\omega t) \\ \frac{dv_{cs}}{dt} &= (\frac{dv_s}{dt} - \omega v_c) sin(\omega t) + (\frac{dv_c}{dt} + \omega v_s) cos(\omega t) \end{aligned}\right\} \tag{18}$$

The streamlined Fourier series expansion of the voltage v_{AB} (taking into account just the first harmonic) may therefore be stated by applying Fourier decomposition expansion to the voltage v_{AB} indicated in "(11)" as :

$$v_{AB} = a_1 sin(\omega t) + b_1 cos(\omega t) \tag{19}$$

The following procedures were used to get the first harmonic of the Fourier coefficients

$$\left.\begin{aligned} a_1 &= \frac{1}{\pi} \int_{\pi}^{2\pi} v_{AB} sin(\omega t)\ d\omega t = -\frac{\pi V_{cc}}{2} \\ b_1 &= \frac{1}{\pi} \int_{\pi}^{2\pi} v_{AB} cos(\omega t)\ d\omega t = \frac{(8-\pi^2)V_{cc}}{4} \end{aligned}\right\} \tag{20}$$

Because the current flowing through the rectifier is dc, the dc coefficient of the complex Fourier series may be used to estimate it accurately [18];

$$|i| = \frac{2}{\pi} i_p \tag{21}$$

$$i_p = \sqrt{i_s^2 + i_c^2} \tag{22}$$

We can express $Sgn(i)$ as:

$$Sgn(i) = \frac{4i_s}{\pi i_p} sin(\omega t) v_f + \frac{4i_c}{\pi i_p} cos(\omega t) v_f \tag{23}$$

The new state vector derived from the aforementioned decomposition of Fourier series expansion had five variables: i.e. x = $[i_s \quad i_c \quad v_s \quad v_c \quad v_f]^t$

In order to generate the large signal model, we substitute (16), (18), (19), and (21), into (11), (12), and (14). separating sine and cosine equations, we arrive at:

$$\left.\begin{aligned} \frac{\pi V_{cc}}{2} &= L_t\omega i_c - L_t\frac{di_s}{dt} - v_s - \frac{4i_s}{\pi i_p}v_f \\ \frac{(8-\pi^2)V_{cc}}{4} &= L_t\omega i_c - L_t\frac{di_c}{dt} - v_c - \frac{4i_c}{\pi i_p}v_f \\ i_s &= c_s\frac{dv_s}{dt} - c_s\omega v_s \\ i_c &= c_c\frac{dv_c}{dt} - c_s\omega v_c \\ c_f\frac{dv_f}{dt} &= \frac{2}{\pi}i_p - \frac{v_f}{R_l} \end{aligned}\right\} \tag{24}$$

B. Steady State Model of CPT System

The partial differential (22) in the large signal model with respect to time is equal to zero in the steady state since there is no fluctuation in the state vector with respect to time. The steady state of i_p and v_f is so as follows:

$$I_p = \frac{\pi v_f}{2R_l} \tag{25}$$

Substitute (23) into (22) yield:

$$\left.\begin{aligned} \frac{dI_s}{dt} &= -\frac{8R_l}{L_t\pi^2}I_s + \omega I_c - \frac{1}{L_t}V_s - \frac{\pi V_{cc}}{2L_t^2} \\ \frac{dI_c}{dt} &= -\frac{8R_l}{L_t\pi^2}I_c - \omega I_s - \frac{1}{L_t}V_c - \frac{(8-\pi^2)V_{cc}}{4L_t} \\ \frac{dV_s}{dt} &= \frac{1}{C_s}I_s + \omega V_c \\ \frac{dV_c}{dt} &= \frac{1}{C_s}I_c + \omega V_s \end{aligned}\right\} \tag{26}$$

by equation (24), the steady-state model for the system can be given as:

$$A_{ss} = \begin{bmatrix} -\frac{8R_l}{L_t\pi^2} & \omega & -\frac{1}{L_t} & 0 \\ -\omega & -\frac{8R_l}{L_t\pi^2} & 0 & -\frac{1}{L_t} \\ -\frac{1}{C_s} & 0 & 0 & \omega \\ 0 & \frac{1}{C_s} & -\omega & 0 \end{bmatrix} \tag{27}$$

$$B_{ss} = \begin{bmatrix} -\frac{\pi V_{cc}}{2L_t} \\ \frac{(8-\pi^2)V_{cc}}{4L_t} \\ 0 \\ 0 \end{bmatrix} \tag{28}$$

C. Small Signal Model of CPT System

The large signal model has to be linearized at the nonlinear model's operating point for the controller design. Setting the (24) to zero and solving for the state variable's variable will yield the operating point:

$$0 = AX_e + BV_{cc} \implies X_e = A^{-1}BV_{cc} \tag{29}$$

By using the Taylor series linearization approach on the large signal model, the small signal model is produced. After that, the state space representation is expressed as:

$$\left.\begin{aligned} \dot{\hat{x}} &= A_l\hat{x} + B_l\hat{u} \\ \hat{y} &= c_l\hat{x} \end{aligned}\right\} \tag{30}$$

where the state, input, and output matrices, respectively, are A_l, B_l, and C_l. The state vector is x, the input vector is u, and the output vector is y. they will be given as:

$$\hat{x} = [\hat{i_s} \quad \hat{i_c} \quad \hat{v_s} \quad \hat{v_c} \quad \hat{v_f}]^t, \quad \hat{u} = \hat{w}, \quad \hat{y} = \hat{v_f}$$

The small signal model was used to create the A_l, B_l, and C_l matrices.

$$B_l = [I_c \quad -I_s \quad V_c \quad -V_s \quad 0]^t$$

$$C_l = [0 \quad 0 \quad 0 \quad 0 \quad 1]$$

$$A_l = \begin{bmatrix} -\frac{4I_{ce}^2V_{fe}}{\pi L_t I_{pe}^3} & \omega_0 + \frac{4I_{ce}I_{se}V_{fe}}{\pi L_t I_{pe}^3} & -\frac{1}{L_t} & 0 & -\frac{4I_{se}}{\pi L_t I_{pe}} \\ -\omega_0 + \frac{4I_{ce}I_{se}V_{fe}}{\pi L_t I_{pe}^3} & -\frac{4I_{se}^2V_{fe}}{\pi L_t I_{pe}^3} & 0 & -\frac{1}{L_t} & -\frac{4I_{ce}}{\pi L_t I_{pe}} \\ \frac{1}{C_s} & 0 & 0 & \omega_0 & 0 \\ 0 & \frac{1}{C_s} & -\omega_0 & 0 & 0 \\ \frac{2I_{se}}{\pi C_p I_{pe}} & \frac{2I_{ce}}{\pi C_p I_{pe}} & 0 & 0 & -\frac{1}{R_l C_f} \end{bmatrix} \tag{31}$$

7. Open loop simulation of the CPT system(without controller)

Given parameters:

Table 2. Given values for the simulation.		
S.No.	**Parameters**	**values**
1.	Input voltage	12 V
2.	Output power	30 W
3.	Q factor	10
4.	resonant frequency	1 MHz
5.	Duty Cycle	0.5

Based on the assumptions and analyses of the CPT System with Class E inverter as described in the previous Section, the system parameters were computed.

- The equivalent resistance, $R_e = \frac{8}{\pi^2+4}\frac{V_{CC}^2}{P_o} = 2.77\Omega.$ and $R_l = \frac{\pi^2}{8}R_e = 3.42\Omega.$
- The resonant inductance, $L_t = L_{ext} + L_{res} = \frac{1.153R_e}{\omega} + \frac{QR_e}{\omega} = \frac{11.153R_e}{\omega} = 4.917\mu H.$
- The shunt capacitance, $C_p = \frac{p_o}{\pi\omega V_{cc}^2} = 10.554289\mu F.$
- The equivalent coupling capacitance or series resonance capacitor, $C_s = \frac{1}{\omega Q R_e} = 5.74567\mu F.$
- The choke inductance, $L_c = 2(\frac{\pi^2}{4}+1)\frac{R_e}{f} = 19.21\mu H$

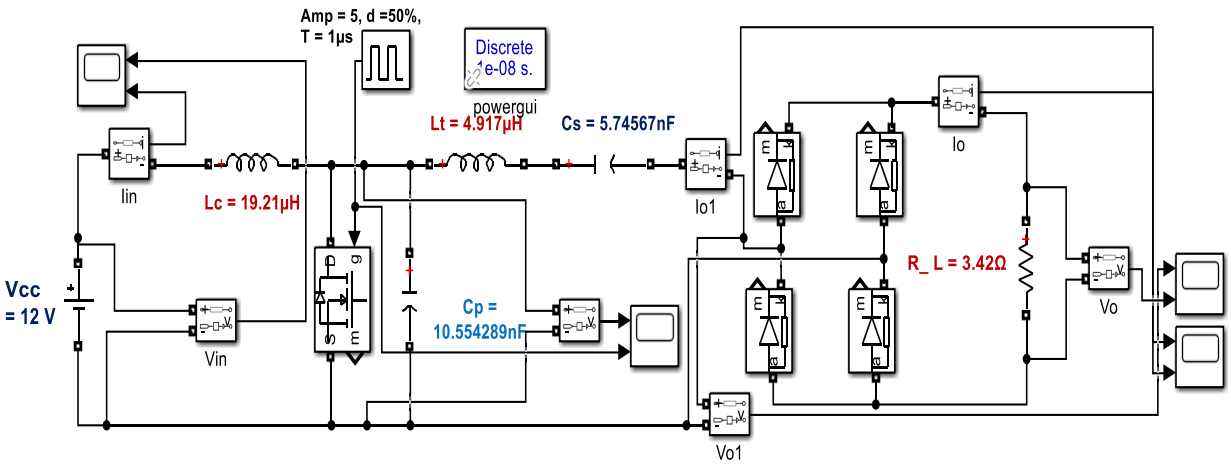

Figure 5: Simulation of CPT model

OBTAINED WAVEFORMS

The waveform of the drain voltage and switching voltage as determined by the simulation is shown in Fig. 3. The graph shows that zero-voltage switching was obtained. The switch voltage is depicted as a square wave with the zero-voltage section in synchrony with the positive half-cycle waveform of the drain voltage, while the drain voltage is shown as a half-cycle waveform.

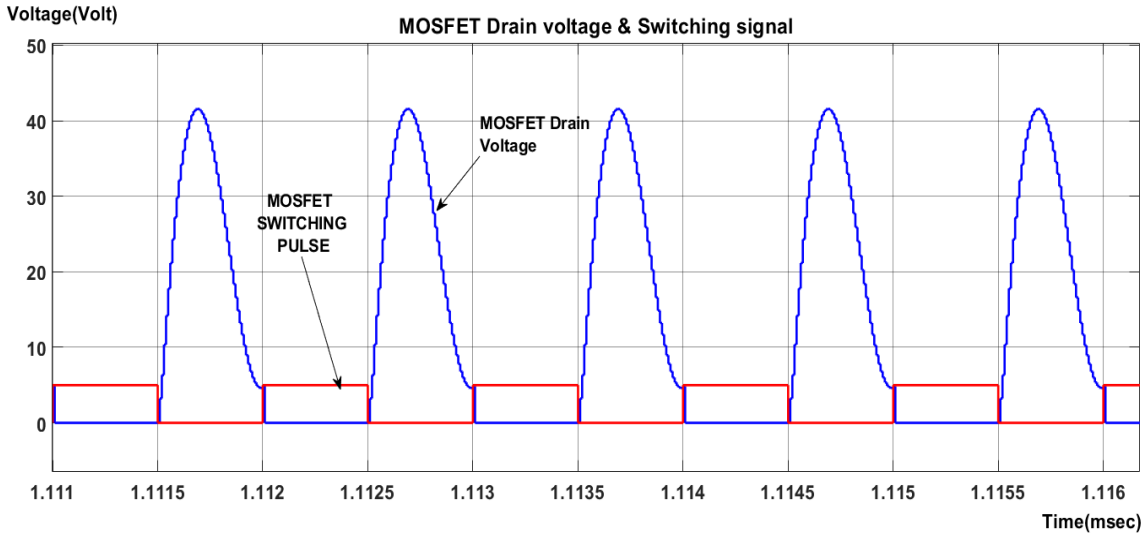

Figure 6: Drain voltage and switch voltage waveforms

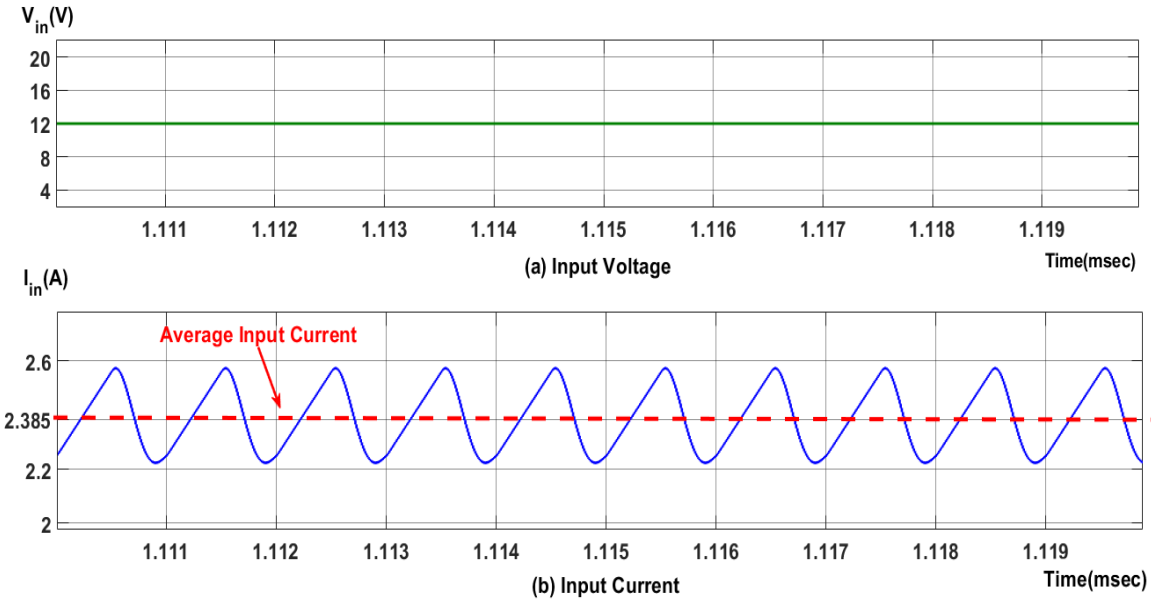

Figure 7: Input voltage and Input Current

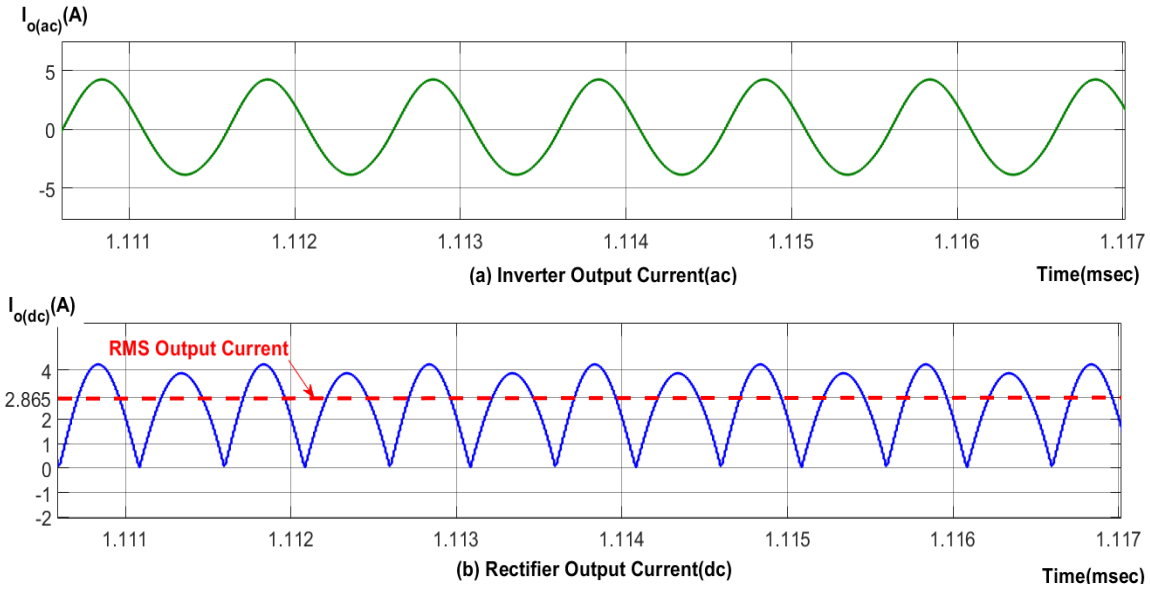

Figure 8: Inverter and rectifier Output currents

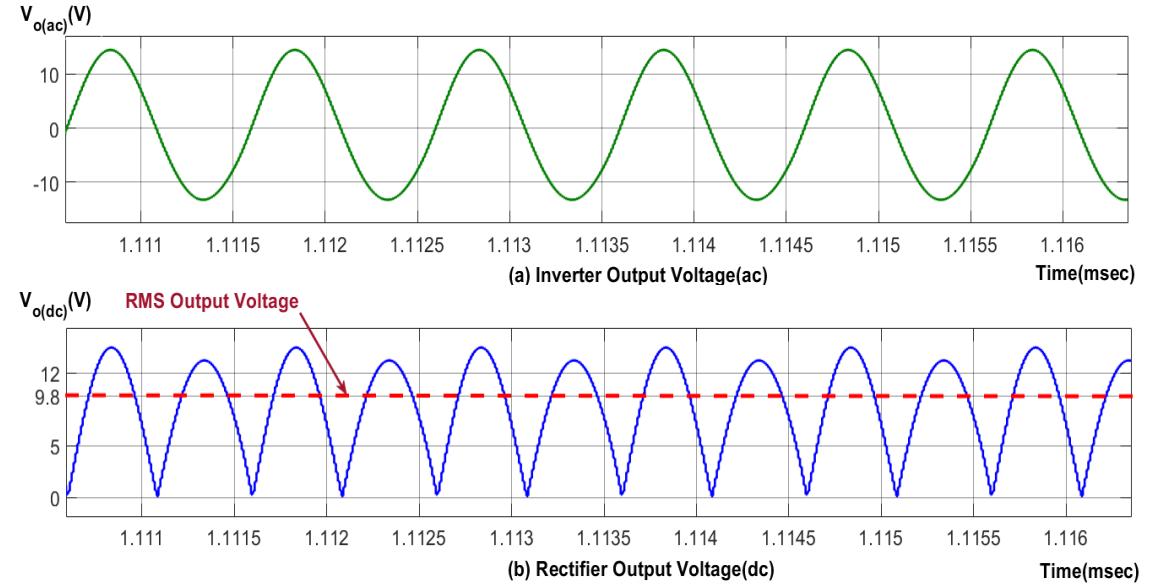

Figure 9: Inverter and rectifier output voltages

Efficiency Calculation:

Obtained Values:

Table 2. Values obtained from the simulation.

S.No.	Parameters	values
1.	Average Input Current	2.385 A
2.	RMS Output voltage	9.8 V
3.	RMS Output Current	2.865 A
4.	Load Resistance	3.42 Ω

Now the Input Power = $V_{in}I_{in} = 12 * 2.385 = 28.62\ W$.
The Output Power = $\frac{V_{rms}^2}{R} = I_{rms}^2 * R = 28.07213\ W$.
The efficiency will be $\eta = \frac{P_o}{P_{in}} = \frac{28.07213}{28.62} * 100\% = 98.15\%$.

8. Conclusions and Discussion

This study analyzed an LCCL CPT system at 1 MHz operating at 98.15% efficiency via simulation. The efficiency of the overall CPT system has been found affected by power losses in the transmitter unit, capacitive coupling distance, and rectifier. This study focused on power losses in the transmitter unit with the aim of enhancing the efficiency of the CPT system. Future work could focus on increasing the efficiency of the system by finding the optimal plate distance for all applications such as biomedical implants, medical applications, and charging space-confined systems such as robots, or mobile devices. In contrast, some research should be carried out in these further areas:

1. Design and optimization of switching devices under high power requirements.
2. The design and optimization of the coupler are suitable for complex environments.
3. Efficient and stable compensation network topology.
4. System efficiency improvement.

References

[1] Y. Awadh and S. Saat, " State Feedback Controller Design for Capacitive Power Transfer System, " 2021 International Congress of Advanced Technology and Engineering(ICOTEN), Taiz, Yemen, 2021,pp. 1- 6, doi10.1109/ ICOTEN52080.2021.9493568.

[2] A. Kumar, S. Pervaiz, C.K. Chang, S. Kor Hummel, Z. Popovic, and K. K. Afridi, "Exploration of Power Transfer density enhancement in Large Air- gap Capacitive Wireless Power Transfer Systems," IEEE Wirel. Power Transf. Conf. WPTC 2015, pp. 1 – 4, 2015.

[3] Y. Yusop, H. Husin, S. Saat, S.K. Nguang, and Z. Ghani, "Class- E LCCL for capacitive power transfer system," in PECON 2016- 2016 IEEE 6th International Conference on Power and Energy, Conference Proceeding, 2017, pp. 428 – 433.

[4] F. Cavalcante and J. Kolar, "Small-Signal Model of a 5kW High Affair Voltage Capacitive- Loaded Series- similar sonorous DC-DC Converter, " in IEEE 36th Power Electronics Specialists Conference, 2005, vol. 52, pp. 1271 – 1277.

[5] S. Sanders, J. Noworolski, X. Liu, and G. Verghese, " Generalized Averaging system for Power Conversion Circuits, " in 21st Annual IEEE Conference on Power Electronics Specialists, 1990, pp. 333 340.

[6] M. Salem, A. Jusoh, N.R.N. Idris, and I. Alhamrouni, "Modeling and Simulation of Generalized State Space Comprising for Series Resonant Motor," in 2014 Australasian Universities Power Engineering Conference (AUPEC), 2014, pp. 1 – 5.

[7] E.X. Yang, F.C. Lee, and M.M. Jovanovic, "Small-Signal Modeling of Series and similar sonorous Mills," in IEEE Applied Power Electronics Conference and Exposition- APEC, 2016, vol. 7, pp. 785 – 792.

[8] S. Wangetal., "Modeling and Control styles of Dynamic Wireless Power Transfer System," in 2017 IEEE Transportation Electrification Conference and Expo, Asia- Pacific (ITEC Asia- Pacific), 2017, pp. 1 – 4.

[9] K. Lu, S.K. Nguang, S. Ji, and L. Wei, "Design of machine frequency Tuning Capacitive Power Transfer System predicated on Class- E2 dc/ dc Motor," IET Power Electron., vol. 10, no. 12, pp. 1588 – 1595, 2017.

[10] K. Lu and S. Nguang, "LQG control of Capacitive Power Transfer System," in 2017 IEEE PELS Workshop on Emerging Technologies Wireless Power Transfer, WoW 2017, 2017, pp. 128 – 132.

[11] W.C. BROWN, "The History of Power Transmission by Wadio swells," IEEE Trans. Microw. Theory Tech., vol. 32, pp. 1230 – 1242, 1984.

[12] Z. Wang, Y. Zhang, X. He, B. Luo, and R. Mai, "Disquisition and operation of Capacitive Power Transfer System A Review," Electronics, vol. 11, no. 7, p. 1158, Apr. 2022, doi10.3390 electronics11071158.

[13] T.M. Mostafa, D. Bui, A. Muharam, R. Hattori, and A.P. Hu, "A Capacitive Power Transfer System with a CL Network for Improved System Performance," 2018 IEEE Wirel. Power Transf. Conf. WPTC 2018, pp. 1 – 4, 2019.

[14] S. Aldhaher, D.C. Yates, and P.D. Mitcheson, "Modeling and Analysis of Class EF and Class E/ F Inverters with Series-Tuned Sonorous Networks," IEEE Trans. Power Electron., vol. 31, no. 5, pp. 3415 – 3430, 2016.

[15] M. Yousefi, Z.D. Koozehkanani, J. Sobhi, H. Jangi, and N. Nasirezadeh, "Effectiveness Analysis of Low Power Class- E Power Amplifier," Mod. Appl. Sci., vol. 8, no. 5, p. 19, 2014.

[16] N. Sokal and A. Sokal, "Class E- A New Class of High- effectiveness Tuned Single- concluded Switching Power Amplifiers," IEEE J. Solid-State Circuits, vol. 3, pp. 168 – 176, 1975.

[17] T. Suetsugu and M.K. Kazimierczuk, "Analysis and design of class E amplifier with shunt capacitance composed of nonlinear and direct capacitances," IEEE Trans. Circuits Syst. IRegul. Pap., 2004.

[18] P. Wang, C. Liu, and L. Guo, "Modeling and Simulation of Full-Bridge Series Resonant Converter predicated on Generalized State Space Averaging," Appl. Mech. Mater., vol. 347 – 350, pp. 1828 – 1832, 2013.